JOURNAL OF COMPUTATIONAL PHYSICS 47, 452–462 (1982)

Quasineutral Hybrid Simulation of Macroscopic Plasma Phenomena

DOUGLAS S. HARNED

Electronics Research Laboratory, College of Engineering, University of California, Berkeley 94720

Received February 10, 1982

A method for solving the quasineutral hybrid plasma equations in two dimensions is presented, using full ion dynamics and inertialess electrons. The method uses a predictor-corrector field solver and is extended to allow plasma-vacuum interfaces of arbitrary shape. A three-region method for treating the plasma-vacuum interfaces makes possible the simulation of slowly evolving phenomena over time scales much longer than the ion cyclotron period. The algorithm is applied to the study of rotational instabilities in theta pinch Vlasov equilibria.

I. INTRODUCTION

Many macroscopic problems in plasma physics are characterized by ion Larmor radii comparable to the scale lengths of the system. For these problems, and for problems involving microinstabilities, a fluid description of the ions is inadequate, and the ions must instead be treated in a fully kinetic manner. Also, as plasma behavior dominated by ion physics generally evolves on time scales much longer than characteristic electron time scales, for many problems it is unnecessary to follow the full dynamics of the electron motion. In addition, when the frequencies of interest are low compared to the ion cyclotron frequency, $\omega < \omega_{ci}$, the effects of high frequency phenomena, such as electromagnetic radiation and waves associated with electron inertia, are generally negligible. These considerations have led to the development of quasineutral hybrid plasma simulation codes. Such one-dimensional hybrid simulations have been performed by Sgro and Nielson [1] for theta pinch implosions and by Byers *et al.* [2] for the study of microinstabilities. Two-dimensional $(r-z)$ simulations of theta pinch implosions have been performed by Hewett [3].

Our hybrid algorithm treats ions as particles and electrons as an inertialess fluid. The Darwin limit of Maxwell's equations (i.e., neglecting the transverse displacement current) is used. The electron momentum equation, with inertial terms neglected, is coupled with Maxwell's equations and the statement of quasineutrality in order to determine the electric and magnetic fields. In Section II of this paper, we describe our two-dimensional quasineutral model which has been applied to ion layer kink instabilities. In Section III, we discuss the extension of this algorithm to problems

0021-9991/82/090452–11$02.00/0

having plasma-vacuum interfaces. In Section IV, we show the application of the method to the study of theta pinch rotational instabilities.

II. Model

In this section we describe the quasineutral model and the basic algorithm used in simulation. Ampere's law may be decomposed into its longitudinal (curl-free) and transverse (divergence-free) parts,

$$\nabla \times \mathbf{B} = \frac{4\pi \mathbf{J}_t}{c} + \frac{1}{c}\frac{\partial \mathbf{E}_t}{\partial t}, \tag{1a}$$

$$0 = \frac{4\pi \mathbf{J}_l}{c} + \frac{1}{c}\frac{\partial \mathbf{E}_l}{\partial t}, \tag{1b}$$

where the subscripts l and t, respectively, refer to the longitudinal and transverse parts of a vector quantity. We assume quasineutrality, setting $n_i = n_e$, which implies $\nabla \cdot \mathbf{J} = 0$. If $\mathbf{J}_l$ vanishes at the boundaries, or if the system has periodic boundaries, then $\mathbf{J}_l = 0$ throughout the system. For the study of low frequency phenomena, the Darwin approximation is made, that is, the transverse displacement current is neglected. Ampere's law then reduces to the simple form

$$\nabla \times \mathbf{B} = (4\pi/c)(\mathbf{J}_e + \mathbf{J}_i), \tag{2}$$

where $\mathbf{J}_e$ and $\mathbf{J}_i$ refer to the electron and ion current densities.

Electrons are treated as a fluid so that their motion is assumed to be described by the electron momentum equation

$$n_e m_e (dv_e/dt) = -en_e(\mathbf{E} + \mathbf{v}_e \times \mathbf{B}/c) - \nabla P_e, \tag{3}$$

where m_e is the electron mass, n_e the electron density, $\mathbf{v}_e$ the electron drift velocity, and P_e the scalar electron pressure. For low frequency modes, electron inertia effects are not important. Therefore, the left-hand side of Eq. (3) is set equal to zero. With the electron current expressed as $\mathbf{J}_e = -en\mathbf{v}_e$ and the assumption of quasineutrality, Eqs. (2) and (3) may be combined to produce an expression for the electric field

$$\mathbf{E} = (1/4\pi n_i e)(\nabla \times \mathbf{B}) \times \mathbf{B} - (1/n_i ec)\,\mathbf{J}_l \times \mathbf{B} - (1/n_i e)\,\nabla(n_i T_e), \tag{4}$$

where T_e is the electron temperature. Equation (4) determines the electric field as a function of the magnetic field, electron temperature, ion current, and ion density. Ion currents and densities are determined by linear weighting (particle-in-cell). The magnetic field is advanced by Faraday's law

$$\partial \mathbf{B}/\partial t = -c\nabla \times \mathbf{E}, \tag{5}$$

and the ion particle positions and velocities are determined by integrating the equations of motion

$$d\mathbf{v}/dt = (q/m_i)(\mathbf{E} + \mathbf{v} \times \mathbf{B}/c), \tag{6a}$$

$$d\mathbf{x}/dt = \mathbf{v}. \tag{6b}$$

Although in this work we are interested primarily in phenomena not requiring dissipation, the algorithm may also be applied to dissipative modes, such as tearing modes, by the addition of a resistive term to the right-hand side of Eq. (3).

A two-dimensional simulation code has been developed using this model. The equations are solved in Cartesian coordinates with no variation in the z-direction (i.e., $\partial/\partial z = 0$). The magnetic field is $\mathbf{B} = B_z\hat{z}$ and the quantities J_z, E_z, and v_z are all set equal to zero. Particle motion is followed by a standard leapfrog integrator. The time advance of field quantities given by Eqs. (4) and (5) is accomplished by a predictor-corrector algorithm. This algorithm, as follows, is similar in form to one used in one-dimensional computations by Byers *et al.* [2]. If the quantities $\mathbf{J}_i^{n+1/2}$, $\mathbf{v}_i^{n+1/2}$, $n_i^{n+1/2}$, $\mathbf{B}^n$, and $\mathbf{E}^n$ are known, the magnetic field is advanced by

$$\mathbf{B}^{n+1/2} = \mathbf{B}^n - (c\,\Delta t/2)\,\nabla \times \mathbf{E}^n. \tag{7a}$$

A prediction is then made for $\mathbf{E}^{n+1}$ and $\mathbf{B}^{n+1}$ by

$$\mathbf{E}_{\text{pred}}^{n+1} = -\mathbf{E}^n + 2\mathbf{E}(\mathbf{J}_i, n_i, \mathbf{B}, P_e)^{n+1/2}, \tag{7b}$$

$$\mathbf{B}_{\text{pred}}^{n+1} = \mathbf{B}^{n+1/2} - (c\,\Delta t/2)\,\nabla \times \mathbf{E}_{\text{pred}}^{n+1}. \tag{7c}$$

Using the predicted fields, a predictor particle move is performed to obtain $n_{i,\text{pred}}^{n+3/2}$ and $\mathbf{J}_{i,\text{pred}}^{n+3/2}$ after which $\mathbf{B}_{\text{pred}}^{n+3/2}$ is predicted by

$$\mathbf{B}_{\text{pred}}^{n+3/2} = \mathbf{B}_{\text{pred}}^{n+1} - (c\,\Delta t/2)\,\nabla \times \mathbf{E}_{\text{pred}}^{n+1}. \tag{7d}$$

Finally, the new electric and magnetic fields are obtained from

$$\mathbf{E}^{n+1} = \tfrac{1}{2}\mathbf{E}(\mathbf{J}_i, n_i, \mathbf{B}, P_e)^{n+1/2} + \tfrac{1}{2}\mathbf{E}(\mathbf{J}_i, n_i, \mathbf{B}, P_e)_{\text{pred}}^{n+3/2}, \tag{7e}$$

$$\mathbf{B}^{n+1} = \mathbf{B}^{n+1/2} - (c\,\Delta t/2)\,\nabla \times \mathbf{E}^{n+1}. \tag{7f}$$

The particle positions can now be advanced to $n + 3/2$ using these new field quantities. The electric and magnetic fields are stored on interlaced grids. Spatial derivatives are determined by four-point operators, e.g.,

$$(\partial E_x/\partial x)_{i+1/2,j+1/2} = [(E_x)_{i+1,j+1} + (E_x)_{i+1,j} - (E_x)_{i,j+1} - (E_x)_{i,j}]/2\Delta x. \tag{8}$$

The algorithm is second-order accurate in time and space. The corrector iteration is necessary to prevent the appearance of large amplitude odd–even oscillations. The time step is limited by a Courant–Friedrichs–Lewy (CFL) condition on the Alfven speed, $\Delta t < (\Delta x/v_A)$, where $v_A \equiv B_0 c/(4\pi n_i m_i)^{1/2}$. An additional constraint on the

time step for stability is $\omega_{ci}\Delta t < 2$; however, in practice the CFL condition is the more restrictive requirement. The algorithm of Eqs. (7) has been successfully applied in a code using doubly periodic boundaries to study kink instabilities in field-reversed ion layers; these results are discussed elsewhere [4].

III. Plasma-Vacuum Interfaces

The preceding algorithm has the disadvantage that it cannot treat properly low density or vacuum regions, where $n_i \to 0$. We desire to avoid the details of sheath regions or describing low density plasma regions with high accuracy, since the quasineutral hybrid model is not well suited for such problems. However, we would like to include the gross effects due to the fields extending into vacuum regions, such as wall stabilization. Additionally, in highly nonlinear problems, density fluctuations may occur which cause low density or vacuum ($n_i \to 0$) regions to arise in a small number of isolated cells. These will cause local violations of the CFL condition which are sufficient to terminate the simulation unless an alternate method can be found for determining the field quantities in these cells. One possible solution is the addition of a low density plasma throughout the vacuum region which maintains sufficient plasma density so that the CFL condition is satisfied. This method, however, does not produce the instantaneous signal propagation that should occur across a vacuum. Additionally, for a highly nonlinear problem, large amplitude waves are likely to occur in the low density region which can still cause the CFL condition to be violated.

It is desirable to use a method to treat vacuum regions that does not involve the monitoring of complicated, moving, plasma-vacuum interfaces. One such method is described by Hewett [3], where the resistivity is varied in moving from the plasma to the vacuum regions in a nonlinear ADI solution. We have developed another way to include vacuum regions by modification of Eqs. (7b) and (7e) in the algorithm of Section II. Two constants, c_p and c_v, are defined so that in the vacuum $c_p = 0$ and $c_v = 1$, while in the plasma $c_p = 1$ and $c_v = 0$. Then Eq. (7b) is replaced by

$$c_p \mathbf{E}_{\text{pred}}^{n+1} + c_v \nabla^2 \mathbf{E}_{\text{pred}}^{n+1} = c_p(-\mathbf{E}^n + 2\mathbf{E}(\mathbf{J}_i, n_i, \mathbf{B}, P_e)^{n+1/2}), \tag{9a}$$

and Eq. (7e) is replaced by

$$c_p \mathbf{E}^{n+1} + c_v \nabla^2 E^{n+1} = c_p(\tfrac{1}{2}\mathbf{E}(\mathbf{J}_i, n_i, \mathbf{B}, P_e)^{n+1/2} + \tfrac{1}{2}\mathbf{E}(\mathbf{J}_i, n_i, \mathbf{B}, P_e)^{n+3/2}). \tag{9b}$$

A grid point is defined to be plasma if $n_i \geqslant n_c$ and vacuum if $n_i < n_c$, where n_c is a cutoff density, as illustrated in Fig. 1. The effect of the modification is that Eqs. (9a) and (9b) solve the plasma equations (Eqs. (7b) and (7e)) in the plasma and then solve $\nabla^2 \mathbf{E} = 0$, the vacuum electric field solution, in the vacuum. The magnetic field is still advanced by Eqs. (7a), (7c), (7d), and (7f). These equations provide values for

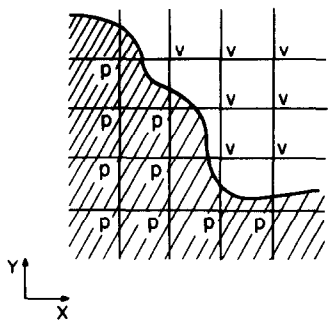

FIG. 1. A schematic of the grid used in the two-region solution. The shaded area corresponds to the plasma region, $n_i > n_c$, and the unshaded region to the vacuum, $n_i < n_c$. In order to calculate the field quantities at a given point, the operator to be applied is determined automatically by whether that grid point is in the vacuum (v) or in the plasma region (p).

B_z in the plasma, in the vacuum, and at the conducting wall. The vacuum field is then smoothed by solving $\nabla^2 B_z = 0$ in the vacuum with the known values of B_z in the plasma and along the conducting wall as boundary conditions. The left-hand side of Eq. (9) is constantly changing as the plasma moves; however, it is solved easily by an iterative matrix solver. Note that no monitoring of the plasma-vacuum interface is required. The CFL constraint is now a condition on the Alfven speed at the density cutoff, n_c. For the magnetic field, this algorithm effectively solves $\nabla^2 \mathbf{A} = 0$ in the vacuum. This method adequately treats fluctuations in low density plasma regions and is capable of handling highly dynamical problems, as well. For the study of slowly evolving plasma behavior, however, such as theta pinch rotational instabilities with growth rates much less than the ion cyclotron frequency, additional care must be taken.

In our two-dimensional model, the theta pinch equilibrium is a cylindrical plasma with an azimuthal current density $\mathbf{J} = J_\theta(r)\,\hat{\theta}$. The initial plasma density is finite at radii $r < r_p$. A vacuum region extends from $r = r_p$ to a conducting wall at $r = r_w$. An axisymmetric theta pinch equilibrium must satisfy the radial force balance equation

$$0 = -\frac{B_z}{4\pi}\frac{\partial B_z}{\partial r} - \frac{\partial P}{\partial r} + n_i m_i r \Omega_i^2, \tag{10}$$

where Ω_i is the mean ion rotational frequency. Near r_p, the first term on the right-hand side of Eq. (10), the magnetic force term, represents the inward force due to magnetic pressure. The other two terms, the thermal pressure term and the centrifugal force term, are both outward near r_p. An equilibrium may easily be set up which obeys Eq. (10) over the bulk of the plasma. Near the plasma-vacuum interface, however, the algorithm of Eqs. (7) and (9) produces diffusion. The reason for this diffusion is that in a region with plasma density below the cutoff density n_c, the magnetic field is constant, because this region is considered to be vacuum and

$\nabla^2 \mathbf{A} = 0$ is effectively solved there (rather than $\nabla^2 \mathbf{A} = 4\pi \mathbf{J}/c$). Since the current is set to zero where $n_c > n_i > 0$, the magnetic force term in this region is also zero. Consequently, the plasma near the interface will diffuse radially because it only sees the outward forces due to the plasma pressure and the centrifugal force of the rotating ions. The error here corresponds to the neglect of the small amount of current density (both ion and electron) carried by the low density plasma, which in the laboratory provides the $\mathbf{J} \times \mathbf{B}$ force that contains the plasma at its edge.

An alternate method for treating plasma-vacuum interfaces has been devised for our two-dimensional simulation code. The plasma is now considered to be in three regions, rather than two. The regions are shown schematically in Fig. 2. The plasma region R_p is still defined to be that with density above n_c. The vacuum region R_v is defined to be that with zero density, or $n_i < n_v$, where n_v is a cutoff value smaller than n_c. The transition region R_t is the region with $n_v < n_i < n_c$. The electric field is solved as described by Eq. (9). The transition region connects the vacuum magnetic field solution with the plasma solution by solving $\nabla^2 B_z = 0$ in R_t with Dirichlet boundaries determined by known plasma and vacuum magnetic fields. For this two-dimensional configuration, the magnetic field at a given time will be uniform throughout the vacuum. Because the simulation region $R = R_p + R_v + R_t$ is assumed to be bounded by a perfectly conducting wall, magnetic flux in the system must be conserved. Therefore, the vacuum magnetic field may be determined by

$$B_z^{\text{vac}}(t) = \frac{1}{A_{\text{vac}}(t)} \left(\int_R B_z(t=0)\, dA - \int_{R_p} B_z(t)\, dA - \int_{R_t} B_z(t)\, dA \right), \tag{11}$$

where A_{vac} is the area of the vacuum region. Generally, the transition magnetic fields are not known until after B_z^{vac} has been computed. Therefore, Eq. (11) is solved iteratively by assuming the transition region to be a vacuum in order to obtain an

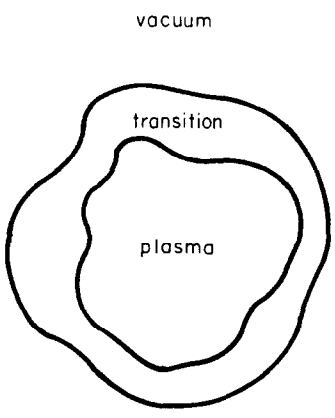

FIG. 2. The three regions for the plasma-vacuum system used in the theta pinch rotational instability problem.

initial estimate for B_z^{vac} at a time step. Then $\nabla^2 B_z = 0$ is solved in the transition region and this solution is substituted back into Eq. (11) to get an improved estimate for B_z^{vac}. This procedure is repeated until total flux conservation is satisfied within a specified convergence criterion.

The effect of this solution on the equilibrium is that the magnetic field now corresponds to that which would be present if the missing current below the cutoff existed in he transition region. If $\partial/\partial\theta = 0$, this current in the transition region is distributed so that the transition azimuthal current density is proportional to $1/r$, since $\nabla^2 B_z = 0$ is solved in that region. The transition region is typically only one or two grid cells in thickness; however, maintaining a finite $\partial B_z/\partial r$ there is critical, as our results demonstrate. Additionally, the small size of the transition region makes the time required for the vacuum and transition magnetic field calculation negligible. Sometimes small internal vacuum regions may occur due to fluctuations which arise in the nonlinear stage of a rotational instability. It is possible to search for such small regions and to handle them as transition cells by solving $\nabla^2 B_z = 0$. The method does not yet appear to be easily applicable to complicated plasma-vacuum interfaces in which large internal vacuum regions exist.

IV. Application to Theta Pinch Rotational Instabilities

We have studied rotating theta pinches starting from exponential rigid rotor Vlasov equilibria [5]. With Ω_e defined as the mean rotational frequency of the electrons, the current density as a function of radius is described by

$$J_\theta(r) = -en_0 r(\Omega_e - \Omega_i)\,\mathrm{sech}^2((r^2 \pm r_1^2)/r_0^2), \tag{12}$$

and the corresponding magnetic field profile is

$$B_z(r) = cm_i\Omega_i^2/e(\Omega_e - \Omega_i) + (c(T_e + T_i)/e(\Omega_e - \Omega_i)\, r_0^2)\tanh((r^2 \pm r_1^2)/r_0^2). \tag{13}$$

The sign preceding r_1^2 in Eqs. (12) and (13) is positive for nonreversed equilibria (i.e., when $B_z(0) > 0$). For $\Omega_i = 0$ or r_1 sufficiently large, a negative sign preceding r_1^2 corresponds to a field-reversed equilibrium (i.e., $B_z(0) < 0$). A parameter α is defined such that $\alpha = -\Omega_i/(\Omega_e - \Omega_i)$. The case $\alpha = 0$ corresponds to a stationary thermal (Maxwellian) ion distribution with all of the current carried by the electrons. This configuration should be stable, according to finite Larmor radius fluid theory [6] and Vlasov-fluid theory [7]. We now demonstrate the difference between the two-region and three-region solutions. Simulations have been performed with a density cutoff n_c at three percent of the peak density. The spatial grid is a 100 by 100 mesh. Fifty thousand particles are used to represent the ions and the time step is $\omega_{ci}\,\Delta t = 0.1$. Figure 3 shows the evolution of the radial density profile (averaged over θ) with time for the two-region solution. The plasma diffusion at the edge eventually leads to the diffusion of the bulk of the plasma, demonstrating that with the two-region solution it is impossible to maintain an equilibrium for times that are long compared to the ion-

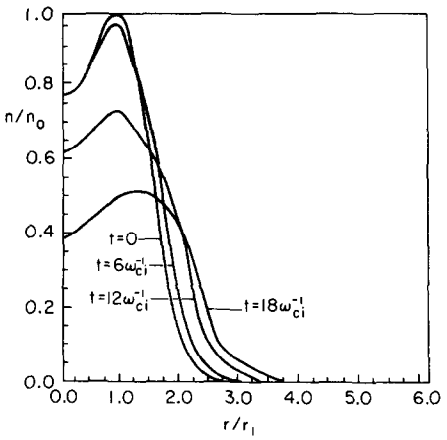

FIG. 3. Theta pinch density profiles, $n_i(r)$, at $t = 0$, 6, 12, and $18\omega_{ci}^{-1}$ for the two-region solution, showing the radial diffusion of the supposedly stable plasma due to the lack of current and the resulting $\mathbf{J} \times \mathbf{B}$ force at the plasma boundary, a numerical defect.

cyclotron period. In contrast, the result for the three-region solution is shown in Fig. 4. The diffusion at the edge has been virtually eliminated and the equilibrium density profile is maintained. It was found possible to reduce the plasma expansion in the two-region solution by using a lower cutoff density; however, since the time step is limited by the CFL condition on the cutoff density, unacceptably small time steps, from an economics standpoint, were required to eliminate the expansion effectively. It may be possible to use a more implicit method, for which the time step is not restricted by the CFL condition at the cutoff density, in order to improve the results of the two-region solution.

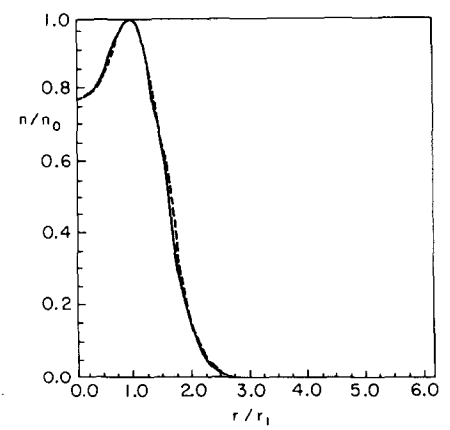

FIG. 4. Theta pinch density profiles, $n_i(r)$, at $t = 0$ (—) and $t = 18\omega_{ci}^{-1}$ (---) for the three-region solution. The diffusion present in the two-region solution has been eliminated and the density profile of the stable plasma is correctly maintained.

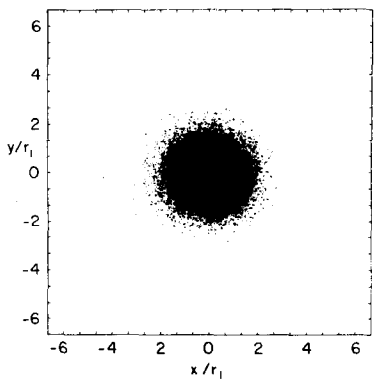

FIG. 5. Initial particle positions for a rigid rotor theta pinch equilibrium.

We have done simulations starting from nonreversed rigid rotor theta pinch equilibria with $\alpha > 0$. These simulations have $(\Omega_e - \Omega_i)/\omega_{ci} = 0.022$ and $\beta_0 = 0.75$. Here β_0 is the *beta-on-axis*, $\beta_0 = n_i(0)\, T/(B_0^2/8\pi)$, where $n_i(0)$ is the initial density at $r = 0$ and B_0 is the magnitude of the external magnetic field. No instabilities have been observed for nonreversed equilibria with $\alpha = 1.0$. For $\alpha = 2.0$, however, an $m = 2$ instability, where m is the azimuthal mode number, is evident. These observations are in agreement with the theoretical predictions of Freidberg and Pearlstein [6] and Seyler [7]. Figure 5 shows the initial ion particle positions for an equilibrium with $\alpha = 2.0$. Seyler [7] predicts the growth rate for this equilibrium to be $(\gamma/\omega_{ci}) = 0.025$ and the real frequency to be $(\omega_r/\omega_{ci}) = 0.033$. The two-region solution is not feasible for this problem because the plasma expansion would obscure the instability on these time scales. Therefore, the three-region method is used. In our simulation, at $t = 144\omega_{ci}^{-1}$, an $m = 2$ instability has grown to large amplitude, as can be seen from the ion particle positions shown in Fig. 6.

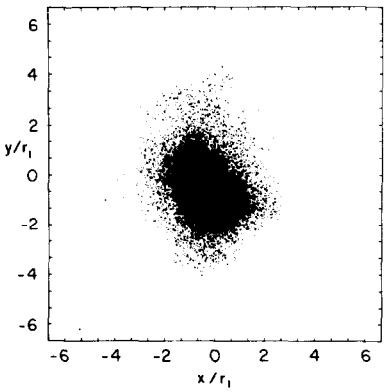

FIG. 6. Theta pinch particle positions at $t = 144\omega_{ci}^{-1}$, after an $m = 2$ instability has grown to large amplitude.

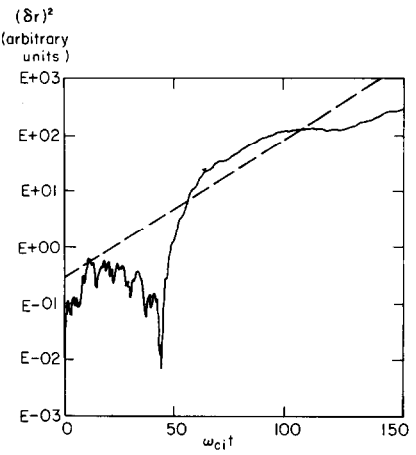

FIG. 7. Values of $(\delta r(t))^2$ for the $m = 2$ mode (—) and the growth rate predicted by Seyler $(\gamma/\omega_{ci} = 0.025)$ (---).

The quantity $\delta r(t, \theta) \equiv \langle r \rangle - \langle r(t = 0) \rangle$ is stored as a diagnostic and decomposed into its azimuthal Fourier components. In Fig. 7 is plotted $(\delta r)^2$ for mode 2, which gives an approximate measure of instability growth. The broken line in Fig. 7 corresponds to $(\delta r)^2$ for the growth rate of Seyler [7] and shows that the growth we observe in our simulation is comparable. We have estimated the real part of the frequency ω_r by measuring the rotation of the elliptically deformed plasma cross section. For this simulation run, we find $(\omega_r/\omega_{ci}) = 0.035 \pm 0.005$. The value determined by Seyler [7], $(\omega_r/\omega_{ci}) = 0.033$, is within the range of error of our simulation estimate.

Although we are studying cylindrical problems with this code, we have observed no spurious numerical effects due to the Cartesian mesh.

V. SUMMARY

A two-dimensional predictor-corrector method for quasineutral plasma simulation, similar to that used in one-dimensional computations by Byers *et al.* [2], has been developed. The method has been extended to allow the inclusion of vacuum and low density regions. A simple, two-region treatment of the plasma-vacuum interface has been found inadequate for the study of instabilities with growth rates much smaller than the ion-cyclotron frequency. For such problems, we have implemented a three-region method of solution which avoids the problems of diffusion at the interface found in the two-region method and avoids time step restrictions associated with following the details of the sheath. The simulation model has been successfully applied to the study of ion layer kink instabilities [4] and theta pinch rotational instabilities.

ACKNOWLEDGMENTS

The author is indebted to Professor C. K. Birdsall for his discussions, advice, and encouragement during the course of this work. Also acknowledged are the many valuable discussions held with Drs. D. W. Hewett, A. Friedman, and B. I. Cohen. This work was supported by ONR Contract No. NOOO14-17-C0578. Computations were performed at the National Magnetic Fusion Energy Computer Center at Livermore.

REFERENCES

1. A. G. SGRO AND C. W. NIELSON, *Phys. Fluids* **19** (1976), 126.
2. J. A. BYERS, B. I. COHEN, W. C. CONDIT, AND J. D. HANSON, *J. Comput. Phys.* **27** (1978), 363.
3. D. W. HEWETT, *J. Comput. Phys.* **38** (1980), 378.
4. D. S. HARNED, Kink instabilities in long ion layers, *Phys. Fluids*, to be published.
5. R. L. MORSE AND J. P. FREIDBERG, *Phys. Fluids* **13** (1970), 531.
6. J. P. FREIDBERG AND L. D. PEARLSTEIN, *Phys. Fluids* **21** (1978), 1207.
7. C. E. SEYLER, *Phys. Fluids* **22** (1979), 2324.